Smart Structures and Systems, *Vol. 27, No. 2 (2021) 397-406*
DOI: https://doi.org/10.12989/sss.2021.27.2.397

Closed loop cable robot for large horizontal workspaces

Sergio Juárez-Pérez [1], Antonio González-Rodriguez [1], Guillermo Rubio-Gómez [1], David Rodríguez-Rosa [1], Erika Ottaviano [2] and Fernando J. Castillo-Garcia*[1]

[1] *Escuela de Ingeniería Industrial y Aeroespacial de Toledo (UCLM), Spain*
[2] *Facoltá di Ingegneria Industriale di Cassino (UNICAS), Italy*

(*Received July 16, 2020, Revised September 28, 2020, Accepted October 10, 2020*)

Abstract. Inspection and maintenance of civil structures are important issues for sustainability of existing and new infrastructures. Classical approach relies on large human activities eventually performed in unsafe conditions. This paper proposed a non-invasive solution for inspecting horizontal surface such as decks of bridges. The proposal presented here is based in cable-driven robots and allows to inspect large surfaces maintaining a very low vertical occupancy in comparison to the conventional architecture of this kind of robot. Using closed cables loop instead of a set of cables a device with low motorization power and very large workspace is designed and prototyped. As example of control an inverse dynamics technique is applied to control the end-effector where inspection tool is located, e.g., a vision system. Experimental results demonstrate that this novel device allows to inspect large horizontal surfaces, with low motorization and low vertical occupancy.

Keywords: cable robot; large workspace; flat large structures; automatic inspection

1. Introduction

In the recent past, a consistent research in the field of Robotics has been devoted to cable-based systems, reflecting the considerable interest according to the large and increasing number of applications. Cable-Driven Parallel Manipulators (CDPMs) use cables to control the end-effector pose, strengthening classic advantages characterizing closed-chain architectures, like large payloads, good dynamic performances, high efficiency, while providing peculiar advantages, such as light weight, large workspace, reduced manufacturing and maintenance costs, deployability and possibility to be moved and mounted on site, superior modularity and reconfigurability (Merlet, book). Moreover, one of the main advantages of CDPMs is that they can be easily adapted to fit certain application or performance requirements, demonstrating greater flexibility than classical robot designs composed by rigid links (Kozak *et al*. 2006, Roberts *et al*. 1998).

The above-mentioned main characteristics of CDPM, mainly related to the very large workspace for positioning, make them very attractive for a many task. One of the first applications dealt with NIST Robocrane (Albus *et al*. 1993) and the systems proposed in Havlik (2000), Nan and Peng (2000), Bosscher (2006). A prototype of a CDPM was developed to be used as suspension system for testing airplane models in wind tunnels, as described in (Yangwen *et al*. 2010). An ultrahigh speed robot design, FALCON-7 was proposed in Kawamura *et al*. (1995) where cables were modeled as non-linear springs taking into account axial flexibility, the model was further developed in Kawamura *et al*. (2000).

Engineering challenges also include material handling over large areas, positioning for heavy objects, rescue operations, service, assistance, rehabilitation, entertainment (Castelli *et al*. 2014) and even the Five hundred meter Aperture Spherical Telescope (FAST), as described in Nan (2006), which is the world's largest filled-aperture radio telescope and the second-largest single-dish aperture after the RATAN-600 in Russia. It consists of a fixed 500 m diameter dish built in a natural depression in the landscape having a novel design, using an active surface made of metal panels that can be tilted by a computer to help change the focus to different areas of the sky. The cabin containing the antenna is suspended by cable. FAST is considered operational nowadays after 3 years testing. The cable mass and sagging effects are not negligible, in this case.

As previously introduced, the most interesting application of CDPM deals with very large workspace, as for the virtual reality simulator (CableRobot Simulator 2020) in which eight supporting cables fully control the motion of a cabin. The design is scalable and can be reproduced in any scale. The IPAnema CDPM was designed for industrial processes (Pott *et al*. 2013).

Cable-suspended camera systems are commonly used in stadiums and arena, they are composed by actuation and transmission systems, most of the time motorized winches and pulleys, which are used to exert or retract cables connected to an end-effector. The end-effector is suspended and consist of a counterbalanced pan and tilt video camera, (Cone 1985, Skycam 2020).

Suspended CDPM is a crane type CDPM in which the end-effector is suspended by n supporting cables, they have attracted the interest of the research community since the

*Corresponding author, Professor,
E-mail: Fernando.Castillo@uclm.es

http://www.techno-press.org/?journal=sss&subpage=7
ISSN: 1738-1584 (Print), 1738-1991 (Online)

workspace is not cluttered by cables and there is less probability of cable interference make them more useful in practical application. Although several works in the literature, the study of these types of robots is still an open field. The major challenge in the position analysis of suspended CDPMs consists of the intrinsic coupling between kinematics and statics (or dynamics). For a fully-constrained CDPM in which the required set of output wrenches is guaranteed with purely tensile cable forces, the posture of the end-effector is determined in a purely geometric way by assigning cable lengths. Instead, for a suspended CDPM, even if the actuators are locked having assigned the cable lengths, the end-effector is still movable; indeed, the equilibrium configuration is determined by the applied forces. Therefore, the end-effector pose (position and orientation) depends on both the cable lengths and equilibrium equations. Moreover, as the end-effector pose depends on the applied external wrenches (forces and torques), it may change due to external disturbances. Therefore, it is necessary considering kinematics together with statics or dynamics equilibrium. The complexity of positioning capability s suspended CDPM is then increased and significantly more difficult than analogous tasks concerning rigid-link parallel manipulators. In the literature, some procedures have been presented, in (Abbasnejad and Carricato 2015) the problem has been defined as geometrico-static also expressing some connections between stability and energy (Carricato and Merlet 2013). The mass and elasticity of cables are taken into account in (Kozak *et al*. 2006, Pott 2010, Merlet 2016). An analytical model is presented for solving the DK and the IK problems of CDPMs with sag cables, based on a mixed formulation of a nonlinear elasto-static problem.

The problem of sagging is much more relevant for suspended CDPM, it has been shown in the literature that the effect in most of those cases cannot be neglected for correct modelling and use of CDPMs (Ottaviano and Castelli 2010, Irvine 1981). Another relevant issue for suspended CDPM is the pulleys that greatly influence the positioning capabilities, in Gonzalez-Rodriguez *et al*. 2017) a solution is proposed for a novel design solution.

In this work a novel design for suspending cable robot is proposed, focused on its optimization for large two-dimensional flat spaces perpendicular to gravity, strictly limiting the occupation in the gravity direction. The proposed cable robot scheme can be used for a great number of tasks carried out in workspaces of these characteristics. Considering the importance for an automatic inspection of large civil infrastructures (Jung *et al*. 2019, Kim *et al*. 2014), authors think that an interesting task for this type of robot would be to inspect the bottom of the large bridges decks (Huang *et al*. 2016) by adding different inspection devices to the end-effector as cameras (Adhikari *et al*. 2016) or laser (Wang *et al*. 2016). In this problem, the space occupied in the vertical direction must be reduced, while the workspace in the horizontal plane is large. Common cable driven suspended robots present serious technical problems when employed in this kind of workspaces, the proposed solution has been specifically designed to solve these problems.

The rest of the paper is organized as follows: Section 2 introduces the novel proposal; Section 3 presents the prototype for experimental validation. Section 4 details the experimental results in term of repeatability and, finally, Section 5 states the main conclusions and further works.

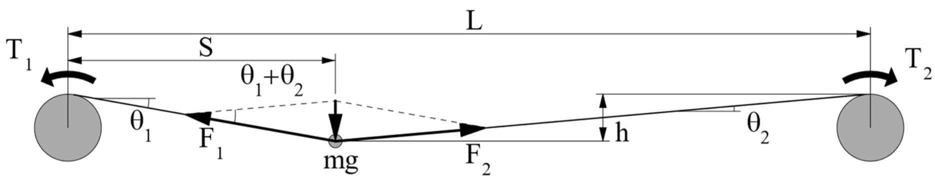

Fig. 1 Forces and torques in a 2D cable robot for a little h

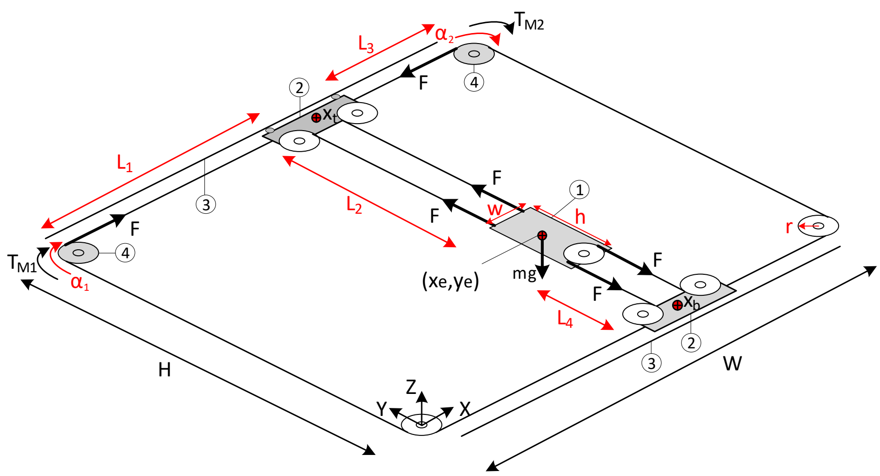

Fig. 2 Proposed 2D cable robot for high workspaces

2. Proposed solution

2.1 Description of the proposal

In cable-driven robots, the end-effector is connected to the frame by several cables. The more extended solution consists on using different cables that join the end-effector to different motors in the frame. Fig. 1 shows a conventional configuration for a suspended cable robot of 2 DOFs. The torque required in each motor is equal to the tension of the cable multiplied by the radius of the pulley or winch joined to the motor.

There are applications for cable robot, such as the inspection of the lower part of bridge decks, in which the workspace must be large in extension, but little space can be occupied in the vertical direction, due to the bridge characteristics. In this case the cable tensions will be very large, even for a light mass m, if L is much greater than h, as shown in Fig. 1.

As an example, if it is required to transport a light mass m = 10 kg with a speed of 1 m/s, for L = 100 m and a vertical occupancy h < 0.2 m, the tension of the cable will be greater than 10 KN for two cables, or greater than 5 kN for four cables. If the cable tension of this robot is high, the torque requirement of the motor is therefore very high, since the diameter of the pulleys has a minimum permissible due to the diameter of the cable. Great torque requirement implies a very high power if the velocity is not near to zero. In this case, the system of Fig. 1 needs 25 kW overall power for moving a 10 kg mass with 1 m/s speed. This represents a disproportionate amount of power.

In order to solve this problem, authors propose employing only one closed cable instead of different cable joined to different motors. The scheme of the proposed robot, along with the nomenclature used in the rest of the paper are shown in Fig. 2. Different elements of the robot shown in Fig. 2 are the end-effector (1), two driving pulleys ((4), grey pulleys) and free pulleys (white pulleys). The robot has also two carriages (2) and two linear guides (3). Cables can replace the guides so that the cars slide through them with new pulleys. (T_{M1}, T_{M2}) are the torques exerted by the left and right motors, respectively, (x_e, y_e) is the end-effector pose, (x_t, x_b) are the x-coordinates of the top and bottom carriages, respectively, (L_1, L_2, L_3, L_4) are the different cable lengths, (α_1, α_2) are the angles turned by the left and right motors, (W, H) are the frame width and height, (w, h) are the end-effector width and height and r is the pulley radius.

Fig. 2 shows the system in a static position. If the end effector is placed in the center of the workspace in the Y direction of movement, the forces will be exactly the same if the cable mass is neglected. If the Z coordinate of the end effector is much less than the distance to either carriages, the forces will be different but very similar. This implies a little reduction in the robot's workspace. Let's call S to the minimum horizontal distance between carriage and end effector, as it shown in Fig.1. The maximum difference between the forces F at both sides of the end effector is given when $L >> S$. In this case $\theta_2 = 0$, F_2 is almost horizontal and ratio F_1/F_2 is

$$\frac{F1}{F2} = \cos\left(\mathrm{atan}\left(\frac{h}{S}\right)\right) \simeq 1 - \frac{1}{2}\left(\frac{h}{S}\right)^2 \qquad (1)$$

In this way, for example, assuming that the end-effector cannot approach less than 10 times the maximum Z coordinate of the end effector, the ratio $1 > F_1/F_2 > 0.995$, and $F_1 - F_2 = 4.9$ N for a vertical force of 98 N.

Another consequence of the proposed approach will be that the tension forces F of the cables will be much greater than the vertical force generated by gravity on the end-effector. Unlike conventional cable robots, this force does not imply high torque in the motors, in fact, for the stationary situation the torque is near zero. The torque in the driven pulleys (4) is null when the end effector is not moving, since the cable does not end in the pulley and tensions in both sides of the pulley compensate each other.

Fig. 3 shows the robot when the end effector is moving with acceleration A in the Y direction. The tension of the four cables of the end-effector is different now, but its difference is only the inertial force required to accelerate the end-effector. For an acceleration of 1 m/s^2 that difference is an order of magnitude less than the gravity force, and several orders of magnitude less than the cable tension.

The torque on the driving pulleys is now $T_M = r\,(F + \Delta F - F) = r\Delta F$. For an acceleration of 1 m/s^2 and a

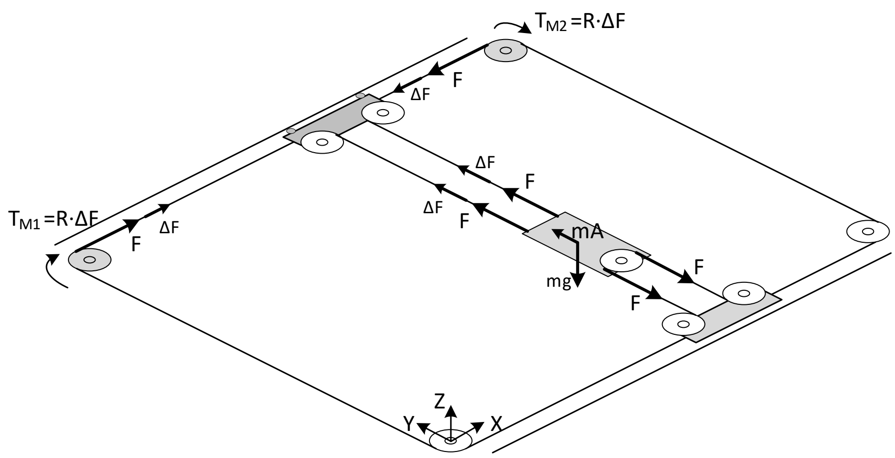

Fig. 3 Proposed 2D cable robot with Y acceleration

speed of 1 m/s it means an output power from the motor of only 10 W, if the friction on the pulley is neglected. This torque is so small that the practical equality between the branches of the cable can no longer be assumed due to a small Z coordinate. But, if this approximation is not neglected, this only adds 5 W more to the previous calculated power. In this way, by correctly choosing the components, the required power will be several orders of magnitude less than the power required for a conventional cable robot where the cable ends in motor pulleys.

The proposed cable robot scheme can be used for a great number of tasks carried out in large two-dimensional flat spaces perpendicular to gravity. The authors think that an interesting task for this type of robot would be to inspect the bottom of the large bridges deck (Huang *et al*. 2016) by adding different inspection devices to the end-effector as cameras (Adhikari *et al*. 2016) or laser (Wang *et al*. 2016). In this problem, the space occupied in the Z coordinate must be reduced, while the workspace in the X-Y axes is large.

Focusing on the workspace characteristics for which the robot has been designed, Fig. 4 shows two alternative schemes proposed for its optimization, as rigid guides are replaced by cables. Several parts of the robots are shown in Fig. 4 as the end-effector (1), the guidance cables (2), driving pulleys (3) and the bridge deck (4). The main dimension of the bridge is along the X-axis.

2.2 Drawbacks caused by friction in the proposed solution and possible solution

In Fig. 5 the proposed system is shown in a dynamic state. In this model the mass is concentrated in the end-effector, and the mass of the carriages is neglected. Dimensions of the end effector and carriage are also neglected compared to the width and the height of the robot frame. Fig. 5 shows a movement in the positive direction of x-axis. The system is represented in three phases of movement: acceleration (a), constant velocity (b) and deceleration (c).

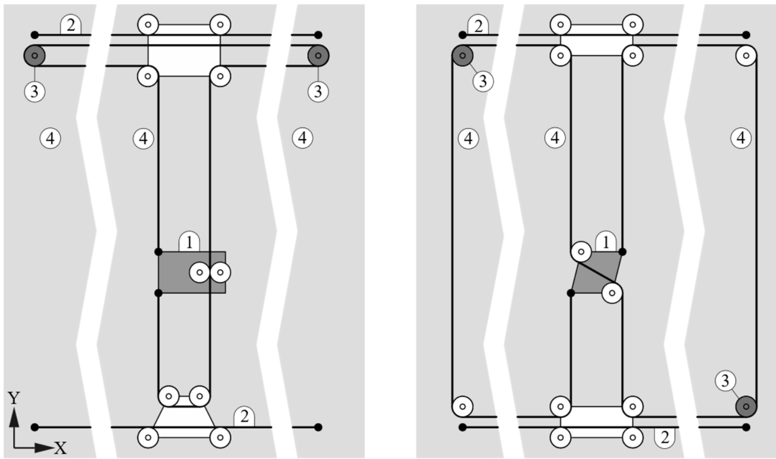

Fig. 4 Alternative schemes for a 2-DOF robot for large spaces

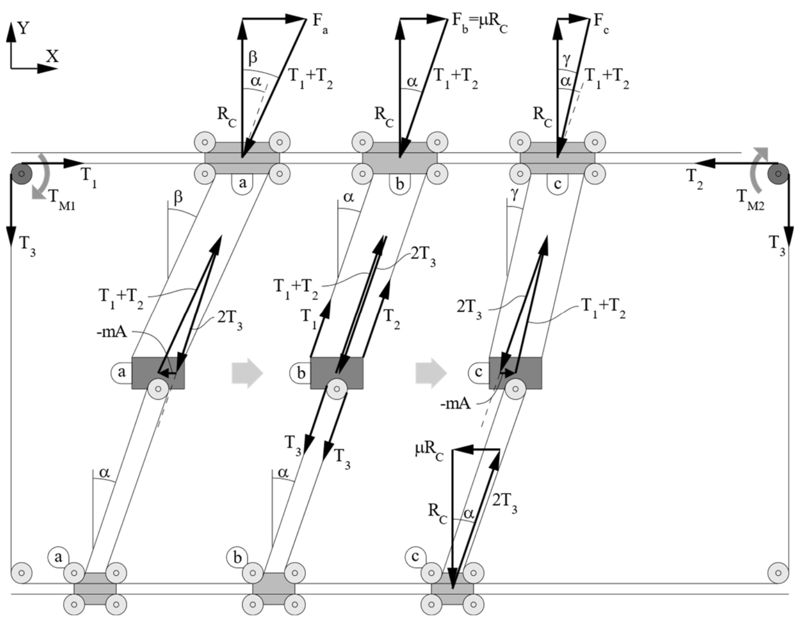

Fig. 5 Proposed 2D cable robot with Y acceleration

In the constant velocity phase the end-effector has no inertial force, therefore the cables that connect them to both carriages must be parallel. This inclination in the carriage cables counteracts the friction force in the guides, with an angle α, as shown in the balance of forces of the carriage labeled as (b). Thus, the horizontal component of the cable tension force is $F_b = \mu R_c$, where μ is the friction coefficient and R_c is the normal reaction force in the carriages given by the guide. This horizontal force F_b is provided by the driving pulleys $F_b = r(T_{M2} - T_{M1})$, where r is the radius of the pulleys and T_{M2} and T_{M1} are the torque of the driving pulleys.

In the acceleration and deceleration forces cables of both sides of the end effector are not parallel in order to counteract the inertial force in the end-effector, as it shown in Fig. 5. Anyway, in the passive branch of the robot (the connected to the free pulleys), the cables always have the same angle α, but in acceleration process the angle of the upper cables is β, while γ is this angle for the deceleration.

The lag in carriage movement is a major problem in maintaining robot positioning accuracy. This is because Coulomb's dry friction would maintain this lag when the carriages had stopped. If the precision is not important for the application of the cable robot, this scheme can be valid, although it would be recommended to maintain carriages friction as low as possible. To solve this problem, the modification of the general scheme shown in Fig. 6 is proposed. In it, two X-cables (a) have been added so that the parallel movement of both cables is forced. This solution presents the problem that with the two carriages located on the same vertical line, the inertial forces in the X direction of the end-effector can only be counteracted by elastic cable extensions.

2.3 Natural frequency of the system

The movement in the Y direction does not present much problem and would be similar than moving a mass on a guide, especially taking into account that the carriage movement is the same thanks to cables (a) in Fig. 6. This is due to the fact that the inertial forces are parallel to the end-effector cables.

Much more problematic is caused by movements in the X direction. Even if the robot application does not need

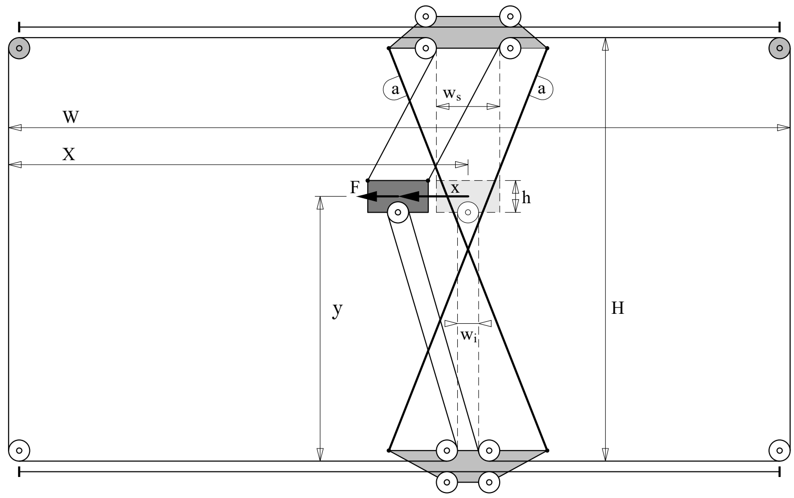

Fig. 6 Proposed solution of increase accuracy in 2D large cable robot

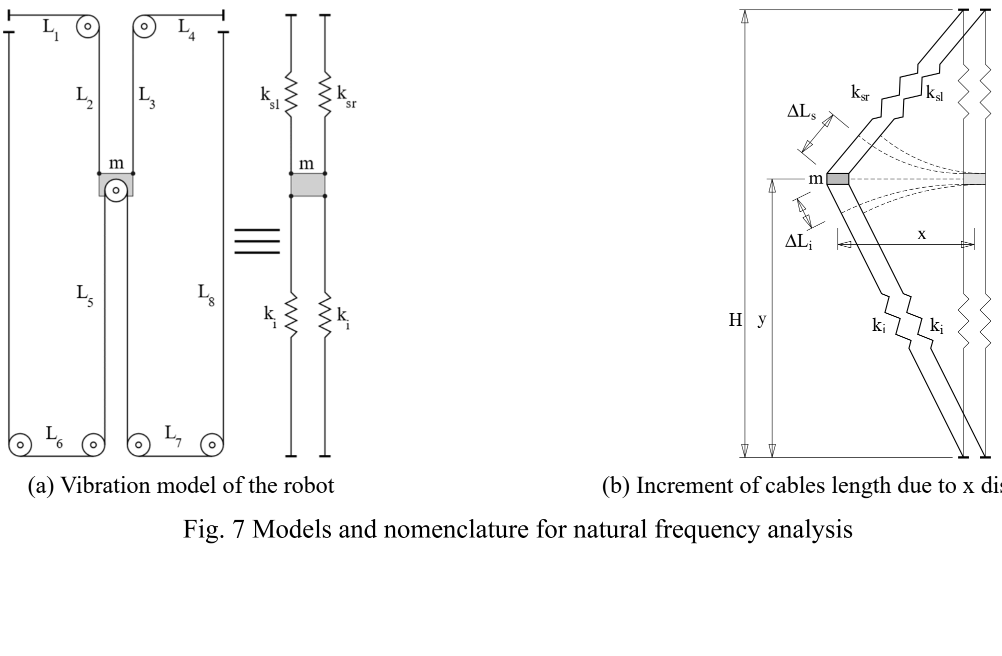

(a) Vibration model of the robot (b) Increment of cables length due to x displacement

Fig. 7 Models and nomenclature for natural frequency analysis high precision, a dynamic model for vibration of the end-effector in the X direction is needed to control the robot. This vibration appears when the end-effector suffers inertial forces in the X direction, even with the motors stopped. The model shown in Fig. 7 will be used for obtaining the dynamic response.

The original scheme can be modeled with the four springs system shown in the right side of Fig. 7(a). The equivalent stiffness of the springs are

$$\begin{aligned} k_i &= 2\left(\frac{2}{k_5}+\frac{1}{k_6}+\frac{1}{k_7}\right)^{-1} \\ k_{sl} &= \frac{k_1+k_2}{k_1k_2} \\ k_{sr} &= \frac{k_3+k_4}{k_3k_4} \end{aligned} \tag{2}$$

where $k_n = (E \cdot A)/L_n$, being E the young modulus of the cable material, A the cross section of the cable and L_n the length of the n-th cable as numbered in Fig. 7(a).

Maintaining a low Z coordinate for the end effector implies the need to pre-stress the robot's cable system. Despite all the cables being connected in a single loop, different prestressing forces could be imposed on the three cable branches if the driven pulleys are actuated. Since the torque of the motor is not comparable to the torque generated by the systems' prestressing, this difference would be lost as soon as the motor of the driven pulleys loses its torque. For this reason, the prestressing will be considered to generate the same force for the three cable branches: the upper two and the lower one.

Dynamic equations will be obtained using Euler-Lagrange formulation and x as generalized coordinate. For obtaining the natural frequency of the system the motor will be considered stopped. The Lagrangian is

$$L = T - U_{sl} - U_{sr} - U_i \tag{3}$$

where

$$\begin{aligned} T &= \frac{1}{2}m\dot{x}^2 \\ U_{sl} &= \frac{1}{2}k_{sl}(\Delta L_s + \Delta L_{Psl})^2 \\ U_{sr} &= \frac{1}{2}k_{sr}(\Delta L_s + \Delta L_{Psr})^2 \\ U_i &= 2\left(\frac{1}{2}k_i(\Delta L_i + \Delta L_{Pi})^2\right) \end{aligned} \tag{4}$$

and where ΔL_i and ΔL_s are the length increment due to x displacement. ΔL_{Psl} , ΔL_{Psr} and ΔL_{Pi} are the length increase due to the prestressing of the cable. F_P is the prestressing of the cable, this force is unique and yields as

$$F_p/k_T = \Delta L_{PT} \tag{5}$$

where

$$\begin{aligned} \Delta L_{PT} &= \Delta L_{Psl} + \Delta L_{Psr} + 2\Delta L_{Pi} \\ k_T &= \left(\frac{1}{k_1}+\frac{1}{k_2}+\frac{1}{k_3}+\frac{1}{k_4}+\frac{2}{k_5}+\frac{1}{k_6}+\frac{1}{k_7}+\frac{2}{k_8}\right)^{-1} \end{aligned} \tag{6}$$

This fact allows calculating the increments of length due to the prestressing.

$$\begin{aligned} F_p/k_{sl} &= \Delta L_{Psl} \\ F_p/k_{sr} &= \Delta L_{Psr} \\ F_p/k_i &= \Delta L_{Pi} \end{aligned} \tag{7}$$

In the other hand, Fig. 6(b) shows the increment of the length of the cables due to the x movement of the mass

$$\begin{aligned} \Delta L_s &= \sqrt{(H-y)^2+x^2} - (H-y) \\ \Delta L_i &= \sqrt{y^2+x^2} - y \end{aligned} \tag{8}$$

where x, y are the end-effector displacement and H the frame height. In this way

$$\begin{aligned} \frac{\partial U_i}{\partial x} &= 2\frac{\partial}{\partial x}\left(\frac{1}{2}k_i\left(\sqrt{y^2+x^2} - y + \Delta L_{Pi}\right)^2\right) \\ &= \frac{xk_i\left(\sqrt{y^2+x^2} - y + \Delta L_{Pi}\right)}{\sqrt{y^2+x^2}} \end{aligned} \tag{9}$$

This derivate can be approximated by Taylor series.

$$\frac{\partial U_i}{\partial x} \cong 2\frac{xk_i\Delta L_{Pi}}{y} + 2\frac{x^3k_i}{2y^2}\left(1 - \frac{\Delta L_{Pi}}{y}\right) + \cdots \tag{10}$$

Cubic terms of the previous expression can be neglected since $x << y$, $x << (H-y)$, $\Delta L_{Ps} << y$ and $\Delta L_{Ps} << (H-y)$. Thus, operating similarly for the upper branch

$$\begin{aligned} \frac{\partial U_i}{\partial x} &\cong 2\frac{xk_i\Delta L_{Pi}}{y} = 2\frac{xF_P}{y} \\ \frac{\partial U_{sl}}{\partial x} &\cong \frac{xk_{sl}\Delta L_{Psl}}{H-y} = \frac{xF_P}{H-y} \\ \frac{\partial U_{sr}}{\partial x} &\cong \frac{xk_{sr}\Delta L_{Psr}r}{H-y} = \frac{xF_P}{H-y} \end{aligned} \tag{11}$$

Now we have all the terms with which to build the Euler-Lagrange equation, with x being the generalized coordinate.

$$\frac{\partial L}{\partial x} - \frac{d}{dt}\frac{\partial L}{\partial \dot{x}} = 0 \Rightarrow m\ddot{x} + xF_P\left(\frac{2}{y} + \frac{2}{H-y}\right) = 0 \tag{12}$$

The natural frequency of the system obtained from equation (x) is

$$\omega_N = \sqrt{\frac{2HF_P}{mY(H-y)}} \tag{13}$$

Expression (13) represents the natural frequency of the system that depends on the y coordinate, the mass of the end-effector and the tension of the cable closed-loop. Fig. 9c, in Section 3, represents the mesh of ω_N values for the entire workspace of the robot compared with the experimental ones for model validation purpose.

2.3 Kinematics model

In this section the robot inverse kinematics model is explained, it allows to compute the angle to be turned by motors to reach an arbitrary end-effector pose. It is employed for the control of the end-effector pose as explained in following sections. Following the nomenclature exposed in Fig. 2 and setting an initial point for the end-effector pose (x_0, y_0), the initial cable lengths can be computed as

$$L_{10} = x_0 - \frac{w}{2}; \qquad L_{20} = H - y_0 - \frac{h}{2}$$
$$L_{30} = W - x_0 - \frac{w}{2}; \qquad L_{40} = y_0 - \frac{h}{2} \tag{14}$$

In a similar manner, cable length for an arbitrary end-effector pose can be computed as

$$L_1 = x_e - \frac{w}{2}; \qquad L_2 = H - y_e - \frac{h}{2}$$
$$L_3 = W - x_e - \frac{w}{2}; \qquad L_4 = y_e - \frac{h}{2} \tag{15}$$

Assuming that the initial angle for the motors corresponds to (x_0, y_0), the inverse kinematics, $[\alpha_1, \alpha_2] = \Lambda^I(x_e, y_e)$, can be obtained

$$\begin{aligned} \alpha_1 &= \frac{1}{r}(L_1 + L_2 - L_{10} - L_{20}) \\ &= \frac{1}{r}(x_e - x_0 + y_0 - y_e) \\ \alpha_2 &= \frac{-1}{r}(L_3 + L_2 - L_{30} - L_{20}) \\ &= \frac{-1}{r}(x_0 - x_e + y_0 - y_e) \end{aligned} \tag{16}$$

3. Experimental platform

3.1 Description

Fig. 8 shows the experimental platform. The frame is made of steel profile and its dimensions are 2.5×2.0 m. The end-effector is 0.35×0.15 m and its weight is 1.2 kg. The upper and downer carriages are mounted on linear guides attached to the frame. The pulleys are made of nylon and their radius is 0.06 m.

The motors are stepper motor Nema 34 (3000 rpm, 27.8 Nm). The position reference is defined by means of

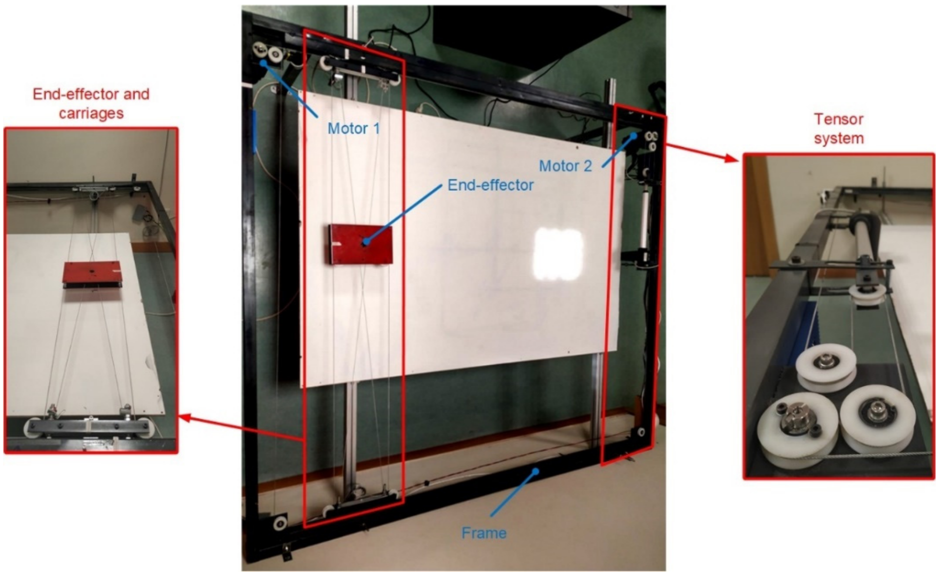

Fig. 8 Experimental platform.

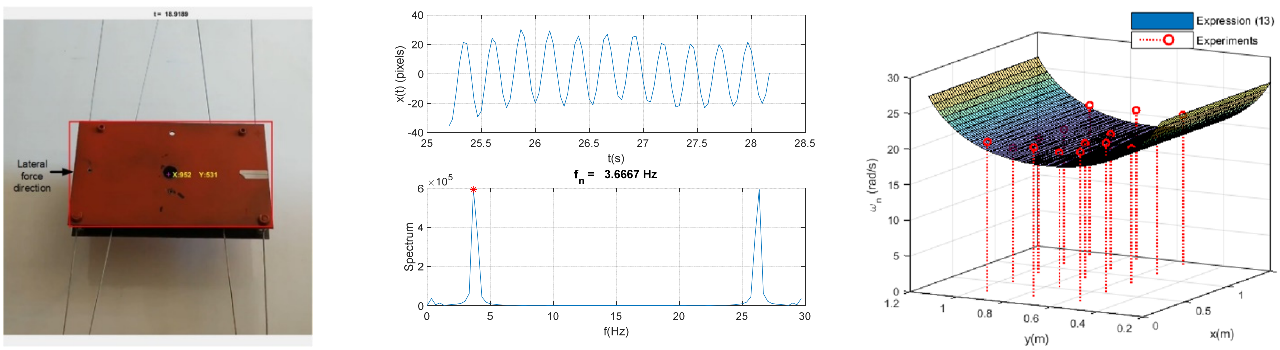

(a) Captured frame for vibration determination

(b) Example of captured movement and natural frequency determination

(c) Natural frequency: model vs. experiments

Fig. 9 Procedure for natural frequency determination a Matlab® application which send the trajectory data to an Arduino Mega controller. This controller commands the movement of the motors by means of two position servocontrollers. The sample time used for the control scheme is 1 ms.

3.2 Frequency domain identification

Expression (13) is an approach to determine the natural frequency of the end-effector. This section details the experimental validation of (13). For a given pose, $[x_e,\ y_e]$ an instantaneous lateral force of 20N is applied to the end-effector on the direction of X axis. A vision system (1080 × 720 p and 60 fps) captures the dynamic image of the end-effector movement. An application developed in Matlab® determines the real word coordinates of the movement of the end-effector. By analysing the displacement of end-effector among X axis, the natural frequency, ω_n, can be determined. Fig. 9(a) shows and example of a captured frame since Fig. 9(b) shows an example of x movement of end-effector after to apply the lateral force, the Fourier Transform of the displacement and the value of an example of natural frequency obtained.

Following this procedure, the natural frequency of the end-effector can be experimentally determined for different end-effector pose and compared to expression (13) for validation purpose (see Fig. 9(c)). The maximum error committed between expression (13) and experiments is less than 10%. Section 4 demonstrates that expression (13) can be successfully applied to implement an easy closed loop for controlling end effector pose.

4. Control approach and results

4.1 Control strategy

Fig. 10 represents the control strategy applied for controlling the proposed device. System dynamics represents the dynamics behaviour of the end-effector when is actuated by means of the stepper motors described in the previous section. In this sense, we are going to consider the dynamics behaviour of the controlled system (inner loop in Fig. 10), is of the form

$$\Psi(s)=\begin{bmatrix}\dfrac{\alpha_1(s)}{\alpha_1^*(s)} & 0\\ 0 & \dfrac{\alpha_2(s)}{\alpha_2^*(s)}\end{bmatrix}=\begin{bmatrix}\dfrac{K_1\omega_{n1}}{s^2+2\xi_1\omega_{n1}s+\omega_{n1}} & 0\\ 0 & \dfrac{K_2\omega_{n2}}{s^2+2\xi_2\omega_{n2}s+\omega_{n2}}\end{bmatrix} \tag{17}$$

being $K_1=K_2=1$ (zero steady state error provided by servocontrollers), $\omega_{n1}=\omega_{n2}$ and equal to the natural frequency identify in Section 3.2 and $\xi_1=\xi_2$ that has been set to 0.4.

The assumption that the inner loop presents a second order and linear dynamics is a strong assumption that is only used as an easy example to control the end-effector pose owing that the actuator system are stepper motors controlled by servocontrollers which dynamics is unknown.

If inner loop is of the form shown in (16), inverse dynamics can be expressed as

$$\Psi^{-1}(s)=\begin{bmatrix}\dfrac{s^2+2\xi_1\omega_{n1}s+\omega_{n1}}{K_1\omega_{n1}} & 0\\ 0 & \dfrac{s^2+2\xi_2\omega_{n2}s+\omega_{n2}}{K_2\omega_{n2}}\end{bmatrix} \tag{18}$$

Although $\Psi^{-1}(s)$ is a non-proper dynamics, it can be precomputed as shown in Fig. 10 in time domain as

$$\begin{aligned}\hat{\alpha}_1^*&=\frac{1}{K_1}\left(\alpha_1^*+2\xi_1\frac{d\alpha_1^*}{dt}+\frac{1}{\omega_{n1}}\frac{d^2\alpha_1^*}{dt^2}\right)\\ \hat{\alpha}_2^*&=\frac{1}{K_2}\left(\alpha_2^*+2\xi_2\frac{d\alpha_2^*}{dt}+\frac{1}{\omega_{n2}}\frac{d^2\alpha_2^*}{dt^2}\right)\end{aligned} \tag{19}$$

This control approach is a simple inverse dynamics technique which use the natural frequency identification of Section 3.2 to generate modified motor angle references, $\hat{\alpha}_1^*$ and $\hat{\alpha}_2^*$, to remove the non-desirable vibration of the end-effector when moves along X-axis.

For ensuring a smooth shape of $\hat{\alpha}_1^*$ and $\hat{\alpha}_2^*$, a third-order trajectory of the end-effector reference has been generated.

4.2 Results

4.2.1 Repeatability

The control approach has been experimentally tested and the end-effector pose, x_e and y_e has been checked by means of the vision system mentioned in Section 3.2.

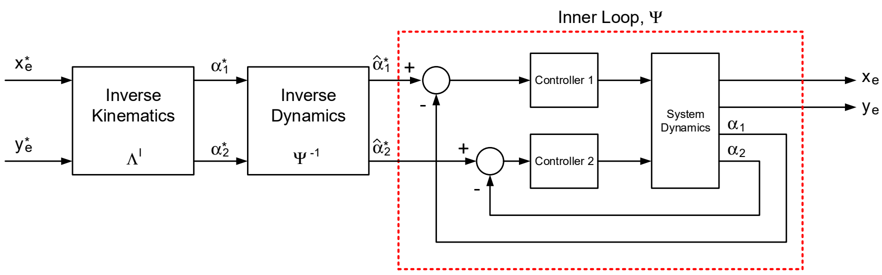

Fig. 10 Experimental platform

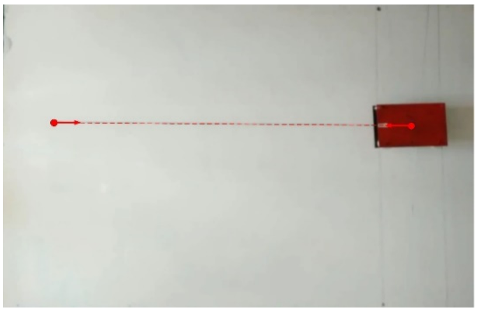

(a) Repeatability test: X-axis movement

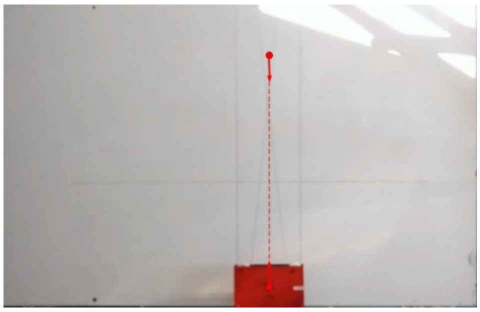

(b) Repeatability test: Y-axis movement

Fig. 11 Repeatability experiments

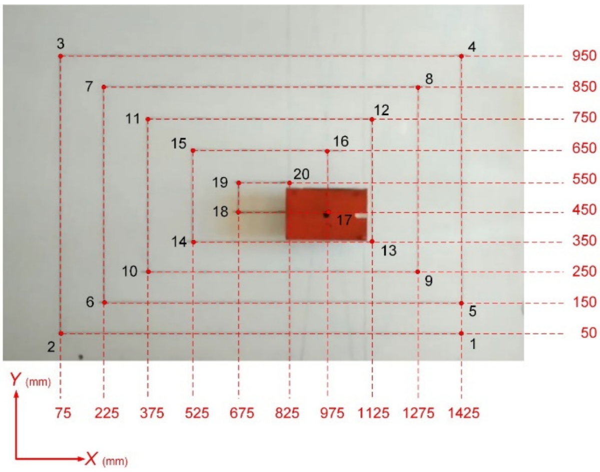

Fig. 12 Trajectory tracking experiment

First results are a related to the robot repeatability. A go and back X and Y-axis trajectories have been repeated 20 times, measuring the error after the 20 manoeuvres. Fig. 11 illustrates the experiments. The error committed for horizontal experiment is 1.6 mm and 0.5 mm for vertical one.

4.2.2 Trajectory tracking

Fig. 12 illustrate the 20-points trajectory executed to check the trajectory tracking of the end-effector.

Table 1 summarizes the steady state error and the maximum following error. Vertical movements naturally present less error than horizontal one. The maximum following error is 14.5 mm (trajectory 15-16) since the maximum steady state error is 2.6 mm (trajectory 18-19).

5. Conclusions

In this work, a novel mechanical design based closed cable loop is presented for inspection of horizontal surface of civil structures. The proposal here is easily scalable for very large workspace maintaining the motorization of the robot. The device presents non-desirable vibration when moving along X-axis. A simple model for determining the natural frequency is developed and experimentally validated. This frequency characterization is applied for controlling the end-effector pose by using an inverse dynamics scheme, owing to the unknown dynamics of the stepper motors-controllers set. The results show that the robot presented here presents an accuracy about 15 mm for trajectory tracking and a maximum steady state error about 2-3 mm.

This proposal is a novel solution to inspect horizontal surfaces if civil structures. This novel device has a low vertical occupancy so it can be considered a non-invasive solution.

Further works in this research line must include the attaching of different inspection systems to the end-effector

Table 1 Trajectory tracking results

Trajectory	Maximum following error (mm)	Steady state error (mm)	Trajectory	Maximum following error (mm)	Steady state error (mm)
1-2	8.9	1.2	11-12	7.5	2.2
2-3	2.1	1.8	12-13	6.2	1.2
3-4	7.2	1.8	13-14	2.5	2.5
4-5	1.8	1.4	14-15	6.0	1.4
5-6	12.4	2.4	15-16	14.5	2.5
f6-7	3.6	2.1	16-17	9.4	1.6
7-8	9.1	2.2	17-18	1.2	1.0
8-9	2.5	1.4	18-19	2.6	2.6
9-10	8.4	1.5	19-20	1.5	0.8
10-11	2.0	1.8			

s cameras or laser to detect, reconstruct and analyse different kind of defects present in horizontal surfaces of civil infrastructures as deck of bridges.

Acknowledgments

The research described in this paper was financially supported by Research Fund for Coal and Steel grant agreement No 800687 in the framework of DESDEMONA project. Authors wish to thank the financial Support provided by the university of Castilla-La Mancha and the European Social Fund through the pre-doctoral funding [2019/451].

References

Abbasnejad, G. and Carricato, M. (2015), "Direct geometrico-static problem of underconstrained cable-driven parallel robots with *n* cables", *IEEE Transact. Robot.*, **31**(2), 468-478. https://doi.org/10.1109/TRO.2015.2393173

Adhikari, R.S., Bagchi, A. and Moselhi, O. (2014), "Automated condition assessment of concrete bridges with digital imaging", *Smart Struct. Syst., Int. J.*, **13**(6), 901-925. https://doi.org/10.12989/sss.2014.13.6.901

Albus, J., Bostelman, Dagalakis, N. (1993), "The nist robocrane", *J. Robot. Syst.*, **10**(5), 709-724.

Bosscher, P. (2006), "Cable-suspended robotic contour crafting system", *Automat. Constr.*, **17**, 45-55. https://doi.org/10.1016/j.autcon.2007.02.011

CableRobot Simulator (2020), "Cable-driven parallel robots – motion simulation in a new dimension", Accessed: 2020-07-10. http://www.ipa.fraunhofer.de/en/cable-driven_parallel_robots.html

Carricato, M. and Merlet, J.-P. (2013), "Stability analysis of underconstrained cable-driven parallel robots", *IEEE Transact. Robot.*, **29**(1), 288-296. https://doi.org/10.1109/TRO.2012.2217795

Castelli, G., Ottaviano, E. and Rea, P. (2014), "A Cartesian cable-suspended robot for improving end-users mobility in an urban environment", *Robot. Comput.-Integr. Manuf.*, **30**(3), 335-343. https://doi.org/10.1016/j.rcim.2013.11.001

Cone, L.L. (1985), "Skycam-an aerial robotic camera system", *Byte*, **10**(10), 122.

Gonzalez-Rodriguez, A., Castillo-Garcia, F.J., Ottaviano, E., Rea, P. and Gonzalez-Rodriguez A.G. (2017), "On the effects of the design of cable-Driven robots on kinematics and dynamics models accuracy", *Mechatronics*, **43**, 18-27. http://dx.doi.org/10.1016/j.mechatronics.2017.02.002

Havlik, S. (2000), "A cable-suspended robotic manipulator for large workspace operations", *Comput. Aided Civil Infrastruct. Eng.*, **15**(6), 56-68.

Huang, T.L., Zhou, H., Chen, H.P. and Ren, W.X. (2016), "Stochastic modelling and optimum inspection and maintenance strategy for fatigue affected steel bridge members", *Smart Struct. Syst., Int. J.*, **18**(3), 569-584. https://doi.org/10.12989/SSS.2016.18.3.569

Irvine, H.M. (1981), "Cable Structures", The MIT Press.

Jung, H.J., Lee, J.H., Yoon, S. and Kim, I.H. (2019), "Bridge Inspection and condition assessment using Unmanned Aerial Vehicles (UAVs): Major challenges and solutions from a practical perspective", *Smart Struct. Syst., Int. J.*, **24**(5), 669-681. https://doi.org/10.12989/sss.2019.24.5.669

Kawamura, S., Choe, W., Tanaka, S. and Pandian, S.R. (1995), "Development of an ultrahigh speed robot falcon using wire drive system", *Proceedings of IEEE International Conference on Robotics and Automattion*, **1**, pp. 215-220.

Kawamura, S., Kino, H. and Won, C. (2000), "High-speed manipulation by using parallel wiredriven robots", *Robotica*, **18**(1), 13-21. https://doi.org/10.1017/S0263574799002477

Kim, C.W., Isemoto, R., McGetrick, P., Kawatani, M. and O'Brien, E.J. (2014), "Drive-by bridge inspection from three different approaches", *Smart Struct. Syst., Int. J.*, **13**(5), 775-796. https://doi.org/10.12989/sss.2014.13.5.775

Kozak, K., Zhou, Q. and Wang, J. (2006), "Static analysis of cable-driven manipulators with non-negligible cable mass", *IEEE Transact. Robot.*, **22**(3), 425-433. https://doi.org/10.1109/TRO.2006.870659

Merlet, J.-P. (2016), "A generic numerical continuation scheme for solving the direct kinematics of cable-driven parallel robot with deformable cables", *Proceedings of IEEE International Conference on Intelligent Robots and Systems*, pp. 4337-4343.

Nan, R. (2006), "Five hundred meter aperture spherical radio telescope (FAST)", In: *Science in China series G*, **49**(2), 129-148. https://doi.org/10.1007/s11433-006-0129-9

Nan, R. and Peng, B. (2000), "A chinese concept for 1km radio telescope", *Acta Astronautica*, **46**(10-12), 667-675. https://doi.org/10.1016/S0094-5765(00)00030-8

Ottaviano, E. and Castelli, G. (2010), "A study on the effects of cable mass and elasticity in cable-based parallel manipulators", *Proceedings of the 18th CISM-IFToMM Symposium, On Robot Design, Dynamics and Control*, Springer Ed. Udine, pp. 149-156.

Ottaviano, E., Arena, A., Gattulli, V. and Potenza, F. (2019), "Slackening effects in 2D exact positioning in cable-driven parallel manipulators", In: A. Pott, T. Bruckmann (Eds.), *Mechanisms and Machine Science*, **74**, Springer, Cham, pp. 319-330.

Pott, A. (2010), "An algorithm for real-time forward kinematics of cable-driven parallel robots", In: *Advances in Robot Kinematics*, Springer, pp. 529-538.

Pott, A., Mütherich, H., Kraus, W., Schmidt, V., Miermeister, P. and Verl, A. (2013), "IPAnema: a family of cable-driven parallel robots for industrial applications", In: *Cable-Driven Parallel Robots* (pp. 119-134), Springer, Berlin, Heidelberg.

Roberts, R., Graham, T. and Lippitt, T. (1998), "On the inverse kinematics, statics, and fault tolerance of cable-suspended robots", *J. Robot. Syst.*, **15**(10), 581-597.

Skycam (2020), Accessed: 2020-07-10. https://en.wikipedia.org/wiki/Skycam

Wang, Q., Kim, M.K., Sohn, H. and Cheng, J.C. (2016), "Surface flatness and distortion inspection of precast concrete elements using laser scanning technology", *Smart Struct. Syst., Int. J.*, **18**(3), 601-623. https://doi.org/10.12989/sss.2016.18.3.601

Yangwen, X., Qi, L., Yaqing, Z. and Bin, L. (2010), "Model aerodynamic tests with a wire-driven parallel suspension system in low-speed wind tunnel", *Chinese J. Aeronaut.*, **23**(4), 393-400. https://doi.org/10.1016/S1000-9361(09)60233-8